Numerical Experiments on the Thermal Equilibrium Temperature in Cirrus Cloudy Atmospheres

By Kuo-Nan Liou and Kristi L. Gebhart

Department of Meteorology, University of Utah, Salt Lake City, Utah 84112, U.S.A.
(Manuscript received 28 September 1981)

Abstract

A number of numerical experiments have been carried out to investigate the climatic effects of the cirrus cloud thickness and location in various atmospheric conditions on the thermal equilibrium temperature of the earth's atmosphere. While the convective adjustment program utilized follows the procedures outlined previously by Manabe and his associates, several new endeavors for treating the transfer of solar and infrared radiation through semi-transparent and nonblack clouds are incorporated into the radiative-convective progarm. The numerical program is developed in such a manner that the solar and infrared radiative properties of cirrus can be carefully treated in conjunction with the temperature profile determination. We show that the presence of a 0.1 km thin cirrus with an infrared emissivity of 0.45 and a solar reflectivity of 0.08 heats the atmosphere by as much as 20°K regardless of the cloud location. However, the influence of thick clouds depends strongly on their atmospheric location. The presence of low thick ice clouds will cool the atmosphere significantly, a conclusion shared by several investigators. A composite thermal equilibrium temperature profile is constructed using the climatological water vapor and ozone profiles and cloud parameters for the tropical atmosphere. Comparison with the climatological temperature profile in the tropics reveal a close agreement (within 1°K) in the troposphere and about 10°K difference in the stratosphere. Using the tropical data, we show that increasing the cirrus cloud cover by 10% at the expense of the clear column will warm the surface temperature by about 0.2°K.

1. Introduction

The most important regulators of the radiation balance are clouds, which absorb and scatter the incoming solar radiation while emitting and absorbing the thermal infrared radiation. Clouds regularly cover about 50% of the sky over the globe. It is apparent that the climatological horizontal extent of the cloud cover and the vertical structure have a very strong impact upon the radiation balance, weather and climate of the earth-atmosphere system. While local variations in cloudiness are a natural and constantly occurring phenomenon due to the changing synoptic-scale conditions embedded in the general circulation, long-term secular changes in cloudiness and vertical structure are difficult to detect. Even with the current satellite sounding technology, means of detecting the compositions and structure of clouds and cloud systems over the globe has not been developed for routine operations and observations.

Although evidence of changes in global average cloudiness does not exist at present, there appears to be evidence that more localized high cloudiness has increased. Machta and Carpenter (1971) reported on secular increases in the amount of high cloud cover in the absence of low and middle clouds at a number of stations in the United States between 1948 and 1970. It has been suggested that there may be a link between the increase in cloud cover and the expansion of jet aircraft flights in the upper troposphere and lower stratosphere in the latitude range between 30° and 65° north (Study of Man's Impact on Climate, 1971). Moreover, cirrus clouds are relatively stable and long-lived, residing as they do in the upper troposphere and lower stratosphere where they are mostly associated with large scale weather disturbances. Thus, the

cirrus cloud climatology could be fairly well determined and significant departures detected once the sounding technique has been developed. Cirrus clouds are composed exclusively of nonspherical crystals having predominant hexagonal structures but with complex shapes also observed. The fact that we see 22° and 46° halos and sundogs proves that cirrus must contain a large portion of oriented hexagonal columns and plates.

In order to understand the climatic impact of high cirrus on the basis of a first order approximation, we have constructed a global radiation budget model with specific emphasis on the cloud and aerosol radiation contributions (Freeman and Liou, 1979). Utilizing the available climatology on the temperature, water vapor, ozone and aerosol profiles and cloud distributions, a zonally averaged radiation balance model was constructed. Several experiments were carried out to investigate the increase of cirrus cloudiness on the heating and cooling in the troposphere and low stratosphere and on the surface temperature. By means of a simple one-dimensional global radiation balance model, it was shown that a 10% increase in cirrus cloudiness, at the expense of clear atmosphere, in the latitude bands from 30° to 60° north latitude leads to a decrease on the global surface temperature by about 1°C.

However, the one-dimensional global radiation model is concerned only with the surface temperature with no vertical resolution or dynamic factor included. The results derived from such a model may not be conclusive and physically reliable. Thus, a second order approximation to understand the climatic effects of cirrus clouds would be to construct a one-dimensional radiative-convective model in which the solar and infrared radiative properties of cirrus can be treated comprehensively in such a manner that the semi-transparent and nonblack characteristics of cirrus could be incorporated in the numerical experiment. For this purpose, we adopt the numerical scheme developed by Manabe and Strickler (1964) and Manabe and Wetherald (1967), known as the convective adjustment, in conjunction with the solar and infrared radiation programs we have developed over the last few years (Freeman and Liou, 1979; Liou and Wittman, 1979; Liou and Ou, 1981) to investigate the cirrus cloud thickness and location and other atmospheric and surface factors on the vertical temperature profile.

In Section 2 of this paper we outline the method for the computation of solar heating rates and fluxes in the atmosphere. A parameterization scheme for computing the infrared fluxes and cooling rates including the radiation contribution of cirrus is then presented in Section 3. A brief discussion on the spirit of the convective adjustment is followed in Section 4. Results and conclusions on the heating and cooling profiles and the thermal equilibrium temperatures due to the variation of cloud parameters and atmospheric conditions are subsequently given in Sections 5 and 6, respectively.

2. Computation of solar heating rate

The basic solar radiation scheme used is based on the plane-parallel model developed by Freeman and Liou (1979) for inhomogeneous atmospheres. It covers the entire solar spectrum in which gaseous absorption is accounted for in scattering layers. Below we outline the procedures involved in the computation of solar fluxes and heating rates. The fundamental transfer equation governing the homogeneous radiation field for the azimuthally independent diffuse monochromatic intensity may be written

$$\mu\frac{dI_\lambda(\tau,\mu)}{d\tau}=I_\lambda(\tau,\mu)-\frac{\tilde{\omega}_\lambda}{2}\int_{-1}^{1}P_\lambda(\mu,\mu')I_\lambda(\tau,\mu')d\mu'-\frac{\tilde{\omega}_\lambda}{4}F_\lambda P_\lambda(\mu,\mu_0)\exp(-\tau/\mu_0), \quad (1)$$

where τ represents the monochromatic optical depth at wavelength λ, μ and μ_0 the cosine of the emergent and solar zenith angles, respectively, and πF_λ the incident solar flux. The single-scattering albedo and the phase function for a layer consisting of both molecules and cloud particles are respectively defined by

$$\tilde{\omega}_\lambda=\frac{\beta_\lambda{}^R+\beta_{\lambda,s}{}^C}{\beta_\lambda{}^R+\beta_{\lambda,s}{}^C+\beta_{\lambda,a}{}^C+\beta_\lambda{}^G}, \quad (2)$$

$$P_\lambda(\theta)=\frac{\beta_\lambda{}^R P_\lambda{}^R(\theta)+\beta_{\lambda,s}{}^C P_\lambda{}^C(\theta)}{\beta_\lambda{}^R+\beta_{\lambda,s}{}^C}, \quad (3)$$

where $\beta_{\lambda,a}{}^C$ and $\beta_{\lambda,s}{}^C$ denote the absorption and scattering coefficients for cloud particles, and $\beta_\lambda{}^C$ and $\beta_\lambda{}^R$ represent the absorption and scattering coefficients for molecules. All four coefficients are in units of per length. The superscripts R and C are abbreviations for Rayleigh molecules and cloud particles, respectively. For a layer without cloud particles, $\beta_{\lambda,a}{}^C=\beta_{\lambda,a}{}^C=P_\lambda{}^C(\theta)=0$.

Utilizing the discrete-ordinates method for radiative transfer, the solutions of the transfer

equation as shown by Liou (1973) are given by

$$I_\lambda(\tau, \mu_i)=\sum_j L_j\phi_{\lambda,j}(\mu_i)\exp(-k_{\lambda,j}\tau) + Z_\lambda(\mu_i)\exp(-\tau/\mu_0), \quad (4)$$

where i and j denote the discrete streams used in approximating the transfer equations, and $\phi_{\lambda,j}$ and $k_{\lambda,j}$ represent the eigenfunction and eigenvalue, respectively. The Z function is associated with Chandrasekhar's H function, the single scattering albedo and the expanded phase function in terms of Legendre polynomials, and the L_j's are coefficients to be determined from the boundary and continuity conditions described below.

To apply Eq. (4) to an inhomogeneous atmosphere, we divide the atmosphere into a number of homogeneous sublayers. At the top of the atmosphere there is no downward diffuse intensity so that

$$I_{\lambda,1}(0, -\mu_i)=0. \quad (5)$$

where $-\mu_i$ indicates that the direction of intensity is downward. Between the sublayers, the intensities from all directions must be continuous and we have

$$I_{\lambda,l}(\tau_l, \mu_i)=I_{\lambda,l+1}(\tau_l, \mu_i), \quad l=1, 2, \cdots, N-1, \quad (6)$$

where N is the total number of sublayers and τ_l is the optical depth from the top of the atmosphere to the layer l. At the bottom of the atmosphere, the upward intensity is given by the reflection of the downward diffuse and direct fluxes as follows:

$$I_{\lambda,N}(\tau_N, +\mu_i)=\frac{r_s}{\pi}\left[2\pi\sum_{i=1}^{n} a_i\mu_i I_\lambda(\tau_N, -\mu_i) + \pi\mu_0 F_\lambda\exp(-\tau_N/\mu_0)\right], \quad (7)$$

where r_s is the surface albedo, a_i the weighting factors, and n the number of discrete streams.

After inserting the intensity solution into the boundary and continuity equations, we obtain a set of linear equations from which the unknown coefficients L_j may be determined by means of a matrix inversion technique. Subsequently, the intensity distribution at any level in the atmosphere may be computed. The monochromatic upward and downward fluxes are given by

$$F_\lambda^{\uparrow}(\tau)=2\pi\sum_{i=1}^{n} a_i\mu_i I_\lambda(\tau, \mu_i),$$

$$F_\lambda^{\downarrow}(\tau)=2\pi\sum_{i=1}^{n} a_i\mu_i I_\lambda(\tau, -\mu_i) + \pi\mu_0 F_\lambda\exp(-\tau/\mu_0). \quad (8)$$

Finally, the upward and downward fluxes at a given height z (or pressure p) covering the entire solar spectrum are

$$F^{\uparrow\downarrow}(z)=\int_0^{\lambda} F_\lambda^{\uparrow\downarrow}(z)d\lambda\approx\sum_{m=1}^{M} F_{\lambda_m}^{\uparrow\downarrow}(z)\Delta\lambda_m, \quad (9)$$

where the solar spectrum is divided into M discrete spectral intervals. The net flux for a given layer may be computed from

$$F(z)=F^{\uparrow}(z)-F^{\downarrow}(z) \quad (10)$$

and the solar heating rate for a layer of air resulting from the absorption by atmospheric gases and/or cloud particles may be calculated from

$$\left(\frac{\partial T}{\partial t}\right)_S=-\frac{1}{\rho C_p}\frac{\partial F(z)}{\partial z}. \quad (11)$$

where ρ is the density and C_p the specific heat at constant pressure.

The primary gaseous absorbers considered in the solar spectrum ranging from 0.2 to 3.2 μm are water vapor, ozone, carbon dioxide and molecular oxygen. The solar spectrum is divided into nine spectral intervals according to the location of absorption bands. Incorporation of water vapor, carbon dioxide and oxygen absorption in scattering atmospheres is accomplished by the exponential fitting of band transmissivities derived by Liou and Sasamori (1975). The fitting program generates a number of equivalent absorption coefficients for each spectral band which are used to evaluate the total optical depth and single-scattering albedo.

3. Computation of infrared cooling rate

In order to compute infrared cooling rates in all weather conditions we have developed a parameterization scheme in which the contribution of nonblack clouds in terms of the broadband radiative parameters is utilized. We consider a cloudy atmosphere containing a semi-transparent and nonblack cloud with the top and base heights denoted by z_t and z_b, respectively. We then derive the cloud broadband infrared emissivity, ε^C, transmissivity, t^C, and reflectivity, r^C, according to the parameterization scheme developed by Liou and Wittman (1979) as follows:

$$R(W)=\sum_{n=0}^{5} C_n W^n, \quad (12)$$

where C_n are the predictor coefficients, W the vertical water/ice content in units of 10^2 g m^{-2}, and R represents ε^C, t^C, or r^C.

In accordance with the geometric configuration

depicted in Fig. 1, we wish to derive the upward and downward fluxes in the atmosphere including the contribution of nonblack clouds in terms of their broadband radiative parameters. For the atmosphere below the cloud, since the gaseous atmosphere is considered to be nonscattering and in local thermodynamic equilibrium, the upward flux at level u is simply given by

$$F^{\uparrow}(u)=\sigma T_s^4+\int_0^u \varepsilon^f[u-u', T(u')]\frac{d\sigma T^4(u')}{du'}du', \tag{13}$$

where the gaseous path length u is related to the height z depicted in Fig. 1, T_s and T are the surface and atmospheric temperatures, respectively, and the broadband emissivity is given by

$$\varepsilon^f(u, T)=\int_0^\infty \pi B_\nu(T)[1-\mathscr{T}_\nu^f(u)]d\nu/\sigma T^4$$
$$\approx\sum_m \pi B_{\bar{\nu}_m}[1-\mathscr{T}_{\bar{\nu}_m}^f(u)]\Delta\nu_m/\sigma T^4, \tag{14}$$

where ν is the wave number, m denotes the number of spectral intervals $\Delta\nu_m$, $\pi B_{\bar{\nu}}$ the spectral Planck flux, and $\mathscr{T}_{\bar{\nu}}^f$ the spectral slab (or diffuse) transmittance. For atmospheric applications, it suffices to introduce a diffusivity constant 1.66 in the flux calculation such that $\mathscr{T}_{\bar{\nu}}^f(u)=\mathscr{T}_{\bar{\nu}}(1.66u)$.

As shown in Fig. 1, the downward flux below the cloud is generated by (1) the reflected flux from layers below the cloud, (2) the transmitted flux from layers above the cloud, (3) the emitted flux from the cloud base, and (4) the atmospheric flux between the layer and the cloud base. Thus, we find

$$F^{\uparrow}(u)=r^c\Big\{\sigma T_s^4[1-\varepsilon^f(2u_b-u, T_s)]$$
$$-\int_0^{u_b}\sigma T^4(u')\frac{d}{du'}\varepsilon^f[2u_b-u-u', T(u')]du'\Big\}$$
$$-t^c\int_{u_1}^{u_t}\sigma T^4(u')\frac{d}{du'}\varepsilon^f[u'-u_t+u_b-u, T(u')]$$
$$\times du'+\varepsilon_b{}^c\sigma T_b^4[1-\varepsilon^f(u_b-u, T_b)]$$
$$-\int_{u_b}^{u}\sigma T^4(u')\frac{d}{du'}\varepsilon^f[u'-u, T(u')]du', \tag{15}$$

where the temperature and path length notations are defined in Fig. 1.

For the atmosphere above the cloud, the downward flux at level u may be expressed by

$$F^{\downarrow}(u)=\sigma T_1{}^4\varepsilon^f(u_1-u, T)$$
$$+\int_{u_1}^{u}\varepsilon^f[u'-u, T(u')]\frac{d\sigma T^4(u')}{du'}du', \tag{16}$$

where T_1 denotes the temperature at the top of the layer, and u_1 is the total path length for the specific gas concerned. The upward flux, like the downward flux below the cloud, is much more involved due to the cloud radiation contribution. It is caused by (1) the reflected flux from layers above the cloud, (2) the transmitted flux from layers below the cloud, (3) the emitted flux from the cloud top, and (4) the atmospheric flux between the layer u and the cloud top. Thus, we find

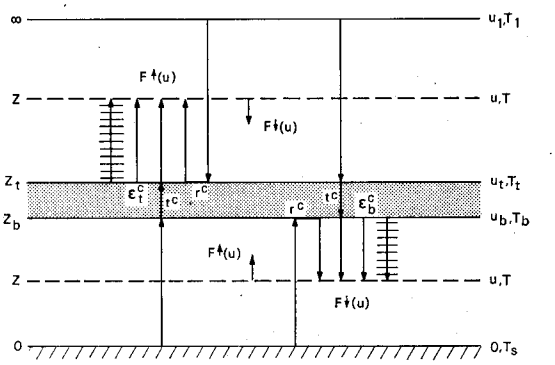

Fig. 1 Configurations of upward and downward fluxes in cirrus cloudy atmosphere.

$$F^{\downarrow}(u)=r^c\int_{u_1}^{u_t}\sigma T^4(u')\frac{d}{du'}\varepsilon^f[u'+u-2u_t, T(u')]du'$$
$$+t^c\Big\{\sigma T_s^4[1-\varepsilon^f(u_b+u-u_t, T_s)]$$
$$-\int_0^{u_b}\sigma T^4(u')\frac{d}{du'}\varepsilon^f[u-u_t-u_b-u, T(u')]du'\Big\}$$
$$+\varepsilon_t{}^c\sigma T_t^4[1-\varepsilon^f(u-u_t, T_t)]$$
$$-\int_{u_t}^{u}\sigma T^4(u')\frac{d}{du'}\varepsilon^f[u-u', T(u')]du'. \tag{17}$$

In the no-cloud condition, $u_b=u_t$, $r^C=\varepsilon^C=0$, $t^C=1$. Equations (15) and (17) reduce to the forms of Eqs. (16) and (13), respectively, after performing integration by parts. On the other hand, if the cloud is an ideal black cloud, $\varepsilon_t{}^C=\varepsilon_b{}^C=1$, $r^C=t^C=0$, Eqs. (15) and (17) also reduce to the forms of Eqs. (16) and (13), respectively, except that the top and surface temperatures are replaced by the cloud bottom and top temperatures, respectively. Once the upward and downward fluxes have been evaluated, the infrared cooling rate at level z may be computed by

$$\left(\frac{\partial T}{\partial t}\right)_{IR}=-\frac{1}{\rho C_p}\frac{dF(z)}{dz}=-\frac{q}{C_p}\frac{dF(u)}{du}, \tag{18}$$

where q is the mixing ratio and the definition of the net flux $F(z)$ is denoted in Eq. (10).

The computation of infrared cooling rates

follows the procedures outlined by Liou and Ou (1981). In that study, five broadband emissivity values corresponding to H_2O rotational, H_2O vibrational-rotational, H_2O continuum, CO_2 and O_3 bands were derived. In conjunction with these broadband emissivity values and the CO_2 and H_2O overlap correction, the upward and downward flux equations, which take into account all the bands, may be derived from the definition of the total broadband emissivity. It is the sum of the emissivity for individual gases minus the emissivity for overlap bands. Subsequently, the total infrared cooling rate may be evaluated.

In accordance with the parameterization scheme developed by Liou and Ou (1981), the broadband emissivities for H_2O, CO_2 and O_3 lines and H_2O continuum were derived from the statistical band model and empirical formula, respectively. Various physical adjustments were performed to incorporate the effects of pressure and temperature on absorption into the gaseous path length. The parameterization scheme involving nonblack clouds simplified the intricate cloud interactions with atmospheric infrared fluxes in terms of the broadband cloud radiative properties. Consequently, the numerical effort and computational time requirement are equivalent to those for clear column cases.

4. Temperature profile determination

The local time rate of change of temperature in the atmosphere is due not only to radiation transfer but also to the upward and horizontal heat transport by atmospheric motions and the latent heat of condensation when clouds are involved. On the basis of the first law of thermodynamics, the rate of the differential increment of heat dq/dt added to a system of gases may be written in the form

$$\frac{dq}{dt}=C_p\frac{dT}{dt}-\alpha\frac{dP}{dt}, \tag{19}$$

where P is the pressure, T the temperature, α the specific volume and C_p the specific heat at constant pressure. In the atmosphere, the rate of energy change per volume $\rho dq/dt$ is caused by the radiation flux divergence in the vertical direction and the latent heat of condensation. Considering only the radiation exchange, Eq. (19) may be rewritten in the form

$$\rho C_p\frac{dT}{dt}-\frac{dP}{dt}=\rho\frac{dq}{dt}=-\left(\frac{dF}{dz}\right)_{\text{rad}}, \tag{20}$$

where the subscript rad denotes the contribution of both solar and thermal infrared radiation. In one dimensional cases, the heating rate, *i.e.*, the local time rate of change of temperature, is given by

$$\left(\frac{\partial T}{\partial t}\right)_{\text{net}}=-\frac{1}{\rho C_p}\left(\frac{dF}{dz}\right)_{\text{rad}}-\omega(\Gamma_d-\Gamma)$$
$$=\left(\frac{\partial T}{\partial t}\right)_{\text{rad}}+\left(\frac{\partial T}{\partial t}\right)_{\text{conv}}, \tag{21}$$

where ρ is the density of air, $\Gamma_d\,(=g/C_p)$ the dry adiabatic lapse rate, $\Gamma\,(=-dT/dz)$ the atmospheric lapse rate, and $\omega\,(=dz/dt)$ the vertical velocity. Thus, a time marching procedure can be devised to obtain the temperature as a function of height (or pressure) as follows:

$$T^{(n+1)}(z)=T^{(n)}(z)+\left(\frac{\partial T}{\partial t}\right)^{(n)}_{\text{net}}\Delta t, \tag{22}$$

where n denotes the index for iterations. Given an initial temperature field, a final steady-state temperature field may be evaluated numerically. Even in a very simple one dimensional case, it is clear that the computation of temperature fields requires the knowledge of the vertical velocity which would involve solving the equations of motion and continuity.

Eq. (21) is derived on the condition that the atmosphere contains no moisture so that the adiabatic lapse rate is given by 9.8°C/km. In a moist atmosphere, the adiabatic lapse depends on pressure and temperature and varies from about 4°C/km near the ground in warm moist air masses to about 7°C/km in the middle troposphere (Wallance and Hobbs, 1977).

To cope with the complexity of computing the velocity field, Manabe and Strickler (1966) and Manabe and Wetherald (1967) proposed a numerical means, now known as the convective adjustment, to derive the vertical temperature profile. Basically, the atmosphere is divided into three categories and a critical lapse rate Γ_c of 6.5°C/km is used from which the atmosphere layer is judged to be convectively stable or unstable. For a non-convective layer we simply have

$$\left(\frac{\partial T}{\partial t}\right)_{\text{conv}}=0 \tag{23}$$

and no adjustment is needed. On the other hand, in a convective layer which is not in contract with the surface, the vertical temperature profile is adjusted to the critical lapse rate Γ_c, subject to the condition that the total potential energy is conserved. That is,

$$\int_{z_b}^{z_t}\rho C_p\left(\frac{\partial T}{\partial t}\right)_{\text{conv}}dz=0, \tag{24}$$

where z_t and z_b denote the top and bottom heights, respectively, of the unstable layer. Physically, this implies that convection develops when the lapse rate exceeds the critical lapse rate; then the convection transports heat upward until the critical lapse rate is established. Consequently, the potential energy is converted to kinetic energy which is eventually dissipated into heat resulting in a redistribution of temperature with total energy conserved. In the event that a convective layer is in contact with the surface, the heating flux from the surface needs to be considered so that

$$\int_0^{z_t} \rho C_p \left(\frac{\partial T}{\partial t}\right)_{\text{conv}} dz = F\uparrow(0), \tag{25}$$

where $F\uparrow(0)$ is a result of the net solar and infrared fluxes.

On the basis of Eqs. (23), (24) and (25), an iterative procedure may be constructed starting from the surface and scanning the layers above progressively and repeatedly at each time step until all layers of super-critical lapse rate have been eliminated. In accordance with the algorithm developed by Manabe and Wetherald (1967), atmospheric temperatures are first constructed based on the balance of radiative heating and cooling rates. Then the surface temperature is derived from the balance of solar and infrared net fluxes at the surface. Since the solar fluxes heat up the surface, there will be net upward fluxes which are to be distributed in the layer above the surface so that Eq. (25) is applicable. Adjusting the temperature stepwise upward using Eq. (24) whenever the layer is convectively unstable eliminates all the supercritical lapse rates.

5. Results

a. Solar heating and infrared cooling rate profiles

In this subsection we first present the broadband infrared and solar radiative properties of clouds. Thicknesses of 0.1, 1, and 3 are used in the calculation and results are depicted in Table 1. A 0.1 km cloud, which contains a vertical ice content of 5.18 g m^{-2}, has an emissivity of about 0.45. While such a cloud may be thought of as a half black cloud, its reflectivity in this case is less than 1% and for all practical purposes its effect may be neglected in the infrared transfer calculation. However, for a 3 km cloud while its emissivity approaches unity, the reflectivity due to effects of multiple scattering has a value of 0.24. Clearly, the high cloud reflectivity will have a considerable influence on the production of warming between the cloud base and the surface. The solar reflection for a 0.1 km thin cirrus when $\mu_0=0.5$ is only about 8.8% with more than 90% of the solar energy transmitting through the cloud. On the other hand, for a 3 km cloud consisting of 156.8 g m^{-2} vertical ice content, the solar reflection increases to about 39%. It should be noted that although the solar reflection (albedo) is only about 9% for the 0.1 km cloud case, such a cloud is already half black in the thermal infrared region. With the large transmitted solar energy coupled with the greenhouse effect produced by the half black cloud, it is conceivable that atmospheric temperatures under the steady-state condition may be increased due to the presence of a thin high cloud. The influence of thin clouds on the atmospheric equilibrium temperature will be discussed in detail in the next subsection. For the intermediate 1 km cloud thickness case, we note that its infrared radiative properties are fairly close to those for the thick 3 km cloud case. But the radiative properties differ greatly in the two cloud cases. The solar albedo, for example, has differences on the order of 15%.

Table 1 Infrared and solar radiative properties of cirrus clouds

	Δz (km)	0.1	1	3
	Δw(g m^{-2})	5.18	51.8	156.8
IR	ε_f	0.449	0.933	0.988
	r_f	0.068	0.188	0.240
	t_f	0.559	0.042	0
SOL	r	0.088	0.237	0.393
	t (μ=0.5)	0.898	0.653	0.425
	α	0.014	0.110	0.182

In Fig. 2 we show the solar heating rate for tropical atmospheres containing 0.1, 1 and 3 km cirrus having a base height of 8 km. The solar heating rate for a clear tropical atmosphere whose humidity and ozone profiles (after McClatchey *et al.*, 1971) are depicted in Fig. 3 is denoted by the solid line. The cosine of the zenith angle μ_0 is taken to be 0.5, representing an approximate average value for a solar day, and the length of the duration of sunlight is assumed to be 12 hrs. For a clear atmosphere the solar heating is ~1°C per solar day in atmospheres below about 10 km due to the absorption of water vapor, whereas in the stratosphere it is produced exclusively by the ozone absorption. Since the heating rate is inversely proportional to the air density, it

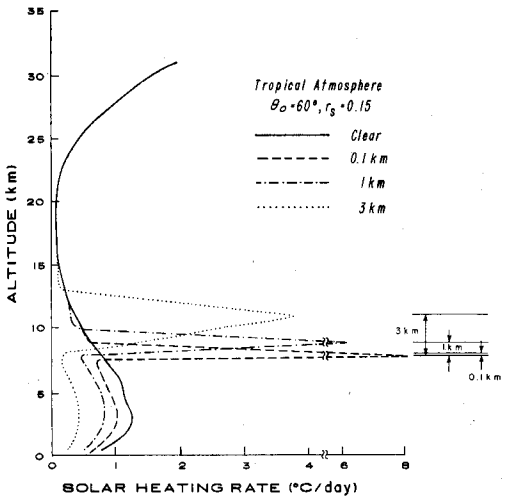

Fig. 2 Solar heating rates in units of °C per solar day for clear and cirrus cloudy atmospheres.

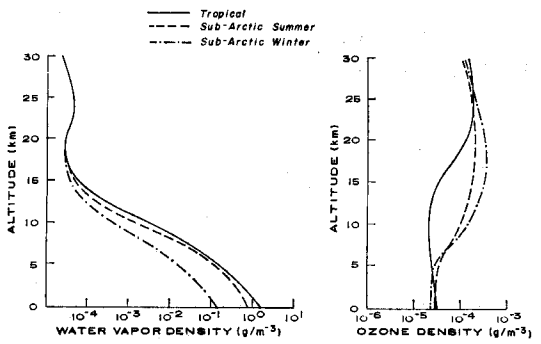

Fig. 3 Water vapor and ozone density profiles for tropical, subarctic summer and subarctic winter atmospheres.

increases drastically in layers above 25 km.

A 0.1 km cirrus generates a heating rate of about 8°C per solar day due to a large difference in the net flux at the cloud top and bottom coupled with a small cloud thickness. Heating rates reduce to 6 and 3°C per solar day for 1 and 3 km thick cirrus, respectively. The reduction of solar heating as the cloud thickness increases is due in part to the finite difference scheme used in the calculation in which the heating rate is inversely proportional to the cloud thickness. The atmospheric heating rates below the cloud decrease as the cloud thickness increases because more solar fluxes are depleted. A 1°C/day reduction is seen for the 3 km cloud case when it is compared with the clear case.

In order to investigate the effects of cloud location on the solar heating rate, additional calculations not presented here were also carried out by lowering the cirrus in the atmosphere. More reduction of the solar heating rate for atmospheres between the cloud and the surface was observed. This is owing to the fact that the solar flux suffers greater attenuation through additional water vapor above the lower cloud. Moreover, the higher the cloud, the greater is the solar heating rate within the cloud layer itself. For the three cloud thicknesses illustrated in this study, a reduction of about 0.5 to 1°C per solar day is obtained when the cloud base is lowered from 8 to 5 km.

The infrared cooling rate profiles for a number of clear and cloudy tropical atmospheres are shown in Fig. 4. The base heights of the clouds are set at 8 km. In a clear tropical atmosphere the infrared cooling profile shows several maxima and minima, in addition to the strong cooling in the upper atmosphere due to carbon dioxide and ozone. The maximum at about 17 km is known as a basic result of the temperature inversion at the tropopause. The maximum at about 10 km and the minimum at about 3 km are associated with the nonlinear interaction of temperature and emissivity slopes. The latter slope is further associated with the water vapor concentration profile. For the case of a 0.1 km cirrus whose emissivity is about 0.45 (see Table 1), more cooling at heights between 16 and 25 km is generated. Below the cloud, the cooling rate is reduced by as much as 1°C/day because of the addition of

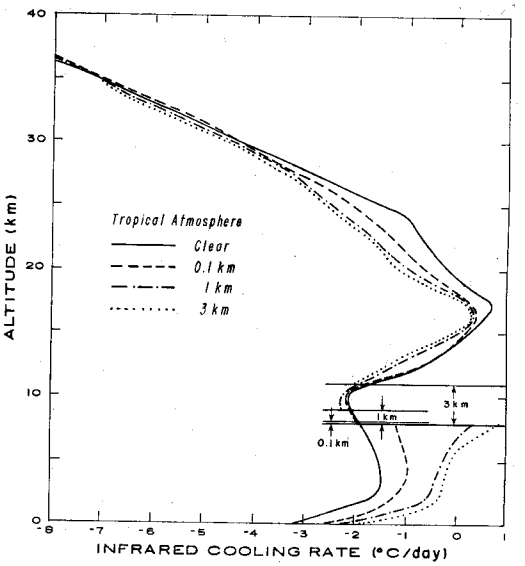

Fig. 4 Infrared cooling rates for clear and cirrus cloudy atmospheres.

the downward flux from cloud emission. The suppression of cooling due to the presence of a half black cloud is indeed significant. In reference to Table 1, we see a significant component of reflected flux from an almost black cloud due to the scattering of infrared radiation by cloud particles. The contribution of reflection and cloud bottom emission produces heating instead of cooling for atmospheres between the cloud bottom and about 5 km height. The reflection component attributes to almost 20% of heating in this case. Atmospheric cooling rates between 20 and 30 km, on the other hand, are enhanced as much as 1 to 2°C/day. Above 30 km, no significant variation of cooling rates is found when a 3 km cirrus is present in the atmosphere. As for the 1 km cirrus case, the cooling rate profile is similar to that for the 3 km cirrus case since the broadband emissivity and reflectivity values for the two cases are about the same as shown in Table 1. The average cooling rate for the 3 km cirrus is about −7.2°C/day.

When the cloud base of a 3 km thick cloud is lowered to 5 km, the atmospheric cooling between the cloud base and the surface is suppressed by about 0.5°C/day. Meanwhile, the average cooling rate for the cloud increases to −8.1°C/day. The physical reason for the cooling suppression is that the lower cloud has a warmer temperature at the cloud base which increases the downward flux from the cloud and consequently heats up the atmosphere below. The larger cooling rate for the lower cloud is an obvious result of the greater net flux difference between the cloud top and base. But it is difficult to pinpoint the exact downward or upward flux component which is responsible for the larger cooling within the cloud. The general trend of lowering the cloud is the reduction of cooling between the cloud and the surface and the increase of average cooling within the cloud.

b. Thermal equilibrium temperatures

Utilizing the radiative-convective program we first carry out a numerical experiment to investigate thermal equilibrium temperatures in clear atmospheres. Three different atmospheric humidity and ozone profiles depicted in Fig. 3 were employed in the calculations. Generally, temperatures below about 15 km are determined by the amount of water vapor. Larger water vapor concentration generates warmer temperatures as illustrated in Fig. 5. This is basically due to the absorption of solar radiation and trapping of

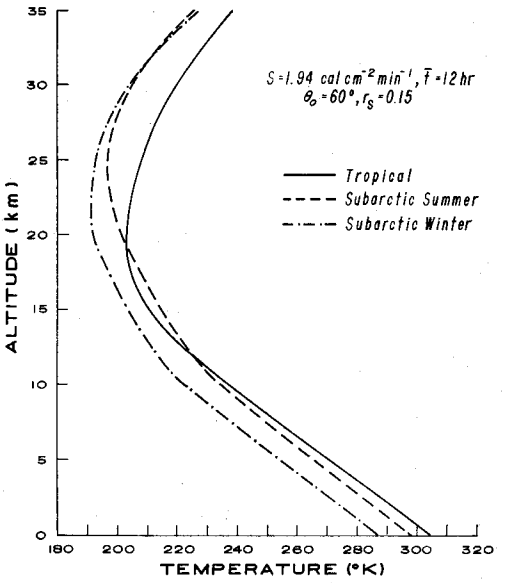

Fig. 5 Thermal equilibrium temperatures in various clear atmospheres.

thermal infrared radiation by water vapor. Above about 15 km the radiative equilibrium temperatures are produced by the balance of the solar heating rate of ozone and infrared cooling of carbon dioxide, ozone and water vapor. Because of the non-systematic distribution of water vapor and ozone profiles used in this study, it is difficult to assess the effects of varying ozone amounts on the equilibrium temperature in the stratosphere.

We next study the influence of the cloud thickness (or ice content) on the temperature profile. Fig. 6 shows the thermal equilibrium temperatures for clear and various cloudy atmospheres using a tropical humidity profile and a surface albedo of 0.15. The cloud base in this graph is placed at 8 km and three cloud thicknesses of 0.1, 1 and 3 km whose radiative properties have been previously described are used in the numerical calculation. Temperatures increase significantly below the tropopause (at ~20 km) when a 0.1 km thin cirrus is inserted in the atmosphere. This is caused by a combination of the large solar energy transmission and the thermal infrared greenhouse effect. The result of the thin high cloud effect on equilibrium temperatures derived in this study is in qualitative agreement with that presented earlier by Manabe and Strickler (1964) and recently by Stephens and Webster (1981). As cloud thickness increases, the atmospheric temperature

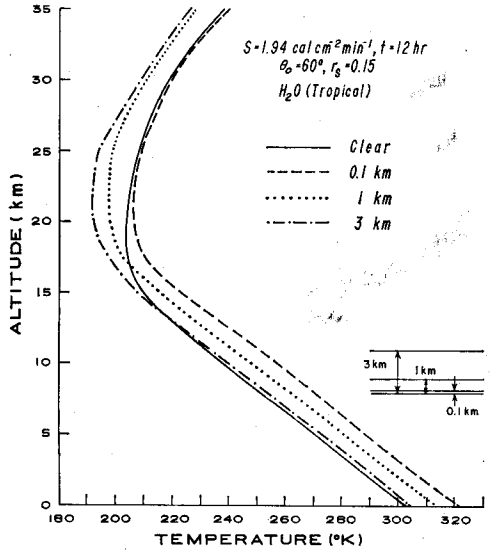

Fig. 6 Effects of the cirrus cloud thickness (or ice content) on the thermal equilibrium temperature. The cloud base is set at 8 km.

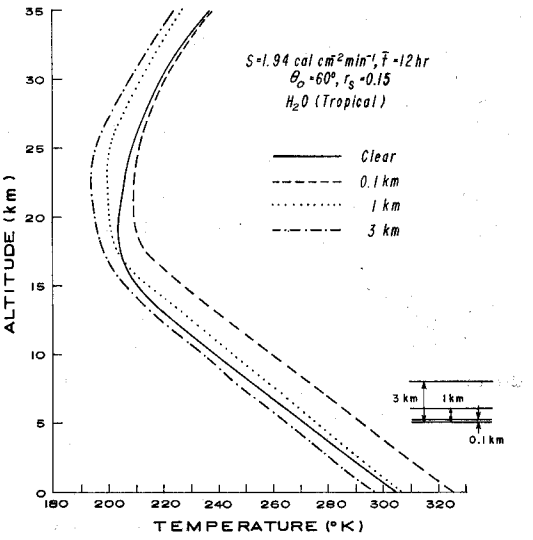

Fig. 7 Effects of the cirrus cloud location on the thermal equilibrium temperature. The cloud base is at 5 km.

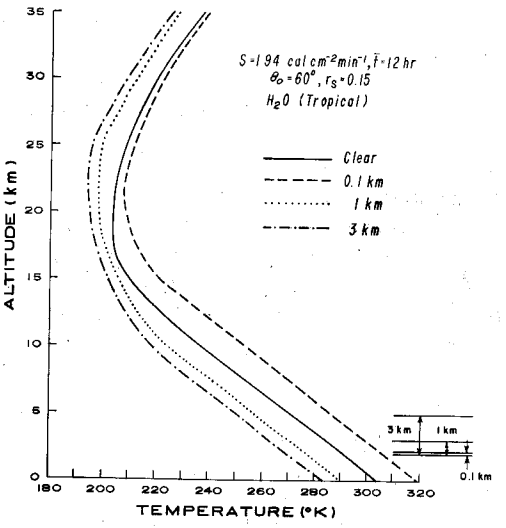

Fig. 8 Same as Fig. 6, except the cloud base is at 2 km.

reduces due to the significant decrease of solar flux. For clouds approaching black bodies, we see colder temperatures above about 15 km. This is because of colder cloud top temperatures acting as surface emitters. Although the difference between the infrared radiative properties for 1 and 3 km cloud cases are rather small, the temperature differences in the two cases are on the order of 10°K below about 15 km due to the difference in the solar radiation properties depicted in Table 1.

The effects of the cloud location in the atmosphere on the thermal equilibrium temperature are shown in Figs. 7 and 8 where the cloud bases are placed at 5 and 2 km, respectively. When the half black thin cloud is lowered from 8 km to 5 and 2 km, equilibrium temperatures vary only slightly. However, when the thick cloud is moved to the lower atmosphere, equilibrium temperatures decrease drastically. For the cloud base in the 5 km case, the presence of a 1 km thick cloud shows small warming with respect to the clear atmosphere. The presence of a 3 km thick cloud, on the other hand, produces cooling everywhere in the atmosphere. When the cloud base is at 2 km, strong cooling takes place in the atmosphere. Below about 15 km, the reduction of the temperatures for a 3 km low cloud is on the order of 20°K. It should be noted that a thick cirrus behaves just like water clouds in the thermal infrared region. However, a thick cirrus has a much lower solar reflection (albedo) than a comparable water cloud having the same thickness. Consequently, we would expect a pronounced reduction of the equilibrium temperature when low water clouds are present in the atmosphere.

In Figs. 9 and 10, we illustrate the effects of the surface albedo on the equilibrium temperature in clear and cloudy atmospheres. We use a subarctic summer water vapor profile and two surface albedos of 0.15 and 0.6 in the numerical

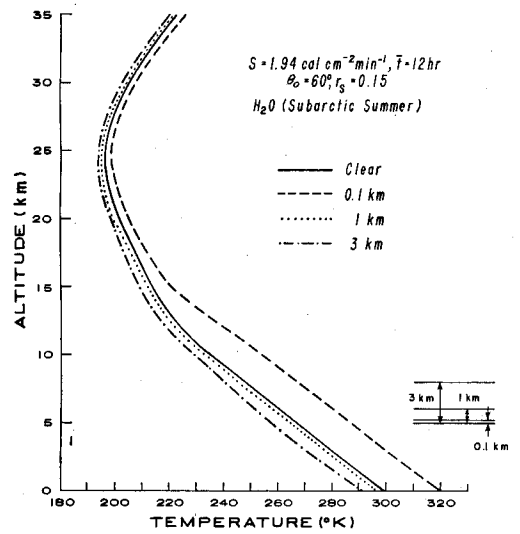

Fig. 9 Thermal equilibrium temperature in a subarctic summer atmosphere using a surface albedo of 0.15. The cloud base is placed at 5 km.

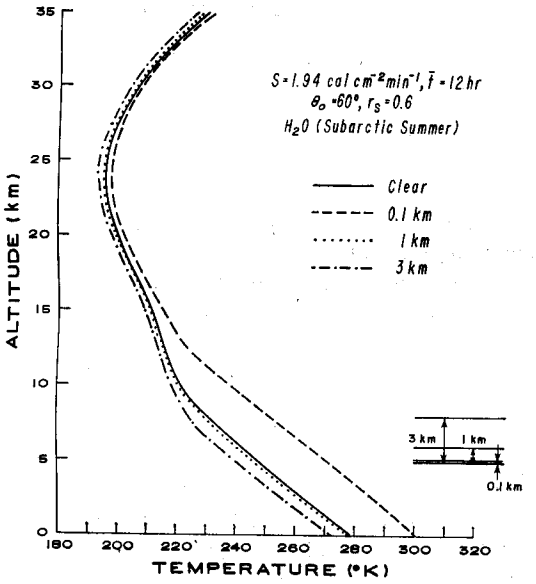

Fig. 10 Same as Fig. 9, except the surface albedo is 0.6. Effects of the surface albedo on the thermal equilibrium temperature.

experiments. The cloud base is fixed at 5 km. For all the cases presented in these two figures, a surface albedo of 0.6 reduces the equilibrium temperature below about 10 km by as much as 20°K. The reason for the colder tropospheric temperature in the case of a higher surface albedo of 0.6 is due to the fact that solar fluxes are reflected back to the atmosphere resulting in a colder surface temperature. And by virtue of the convective adjustment, the colder surface temperature in turn affects the temperature profile with a fixed lapse rate of 6.5°C/km. However, the results presented here correspond to a specific water vapor profile with two surface albedo values and limited cloud thicknesses. Thus, comprehensive and definitive effects of surface albedo on the temperature field in relation to the cloud thickness, cloud height, and cloud type require additional numerical experiments.

Moreover, we wish to investigate the quantitative influence of cloud thickness and location on the surface temperature. As illustrated in Table 2, introduction of a half black high thin cirrus cloud causes the surface temperature to increase significantly. This is basically caused by the additional emission from the cloud. As the cloud thickness increases, the surface temperature decreases but it is warmer than that in the clear case. As the cloud moves to the lower atmosphere, thick clouds produce cooling effects relative to the clear case. Basically, this is due to the fact that only limited water vapor is available for the greenhouse effect to be effective between the cloud base and surface, which in turn affects the surface temperature. For a thin cloud of 0.1 km, when the cloud base moves from 8 km to 2 km the surface temperature first increases then decreases. There appears to be an optimal location in the atmosphere where the half black thin cloud will produce a maximum temperature. For thick clouds, it is rather clear that the surface temperature reduces as the cloud base approaches the surface.

The final experiment is designed to test whether the radiative-convective program presented in the previous sections could accurately reproduce climatological temperature profiles if average conditions of cloudiness are simulated. For this purpose we select a tropical atmosphere and consider six cloud types consisting of low, middle, cirrus, nimbostratus, cumulonimbus and

Table 2. Effects of the cirrus cloud thickness and height on the surface temperature (°K).
(Tropical H_2O, $\mu_0=0.5$, $r_s=0.15$, $\bar{t}=12$ hr).

z_b (km) \ Δz (km)	0	0.1	1	3
8	303.6	321.4	313.3	305.2
5	303.6	324.6	305.0	297.3
2	303.6	318.6	289.7	282.5

Table 3. Cloud base and top heights and fractional cloudiness for each cloud type in a tropical atmosphere

Cloud Type	Cloud Base (km)	Cloud Top (km)	Fractional Cloudiness
low	1.80	2.75	0.129
middle	4.10	5.15	0.061
Ci	10.20	11.90	0.150
Ns	1.48	4.21	0.051
Cb	1.80	6.12	0.035
St	1.48	1.58	0.072
clear	—	—	0.502

stratus. The cloud top and base heights were based on values given by Telegadas and London (1954). The fractional cloudiness for each cloud type was based on the results presented by London (1957) for northern hemisphere and by Sasamori, *et al.* (1972) for southern hemisphere. The mean climatological values of fractional cloudiness, solar zenith angle and surface albedo as presented by Freeman and Liou (1979) were computed by averaging the latitudinal values for 30°S to 30°N taking into account the appropriate surface area. The final averaging was done for the January and July values to obtain the annual condition. The final surface albedo and solar zenith angle used are 0.15 and 0.5, respectively. The cloud height and fractional cloudiness values derived are listed in Table 3.

Except cirrus, all clouds were considered to be black in the infrared radiative transfer calculation. The radiative-convective program was run for each cloud type to obtain the corresponding temperature profile. The composite temperature was then obtained by summing the temperature profile for each cloud type multiplied by the appropriate fractional cloudiness.

Fig. 11 shows the comparison of the computed temperature profile with the climatological tropical temperature profile. From the surface up to 14 km, the difference between the climatological and the simulated temperature is no greater than slightly over 1% for any layer. The surface temperature derived from the numerical experiment is 299.8°K which is only two tenths of a degree different from the climatological value of 300°K. From about 15 km and higher, however, the discrepancy is much larger. The differences near the tropopause can be partially attributed to the convective adjustment program which linearly interpolates temperature between discrete levels. Using the simulated temperature profile as a base we then increase the cirrus cloud cover

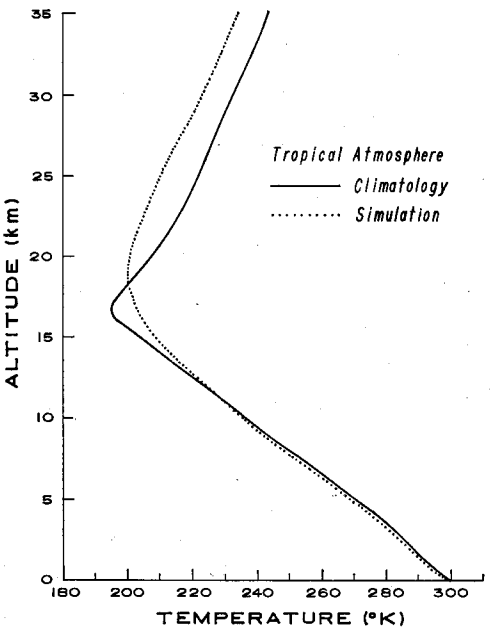

Fig. 11 A simulated thermal equilibrium temperature profile using the cloud climatological data depicted in Table 3. Also shown is the climatological temperature profile for the tropics given by McClatchey, *et al.* (1971).

by 5, 10 and 20% at the expense of the clear atmosphere and compute the equilibrium surface temperature. Subject to the cirrus height and thickness depicted in Table 3, it is found that the surface temperature increases by about 0.1, 0.2 and 0.4°K, respectively.

Additional numerical experiments also have been carried out to derive the vertical temperature profile using the climatological data of water vapor, ozone and cloud parameters for mid-latitude and subarctic atmospheres. Comparisons of the computed and climatological temperature profiles not presented here reveal less satisfactory results as compared with the tropical case. For example, the surface temperature computed for the subarctic summer atmosphere is 4°K colder than the climatological value of 287°K. Differences between the computed and climatological temperatures are generally within about 4-5°K in the troposphere, while in the stratosphere a consistent difference of about 10°K prevails as in the case of the tropical atmosphere. Clouds undoubtedly are the most prominent features which regulate the atmospheric temperature field as clearly illustrated in foregoing experiments. While the cloud data cited herein are the only

source that has been available, their reliability and accuracy are certainly in question. Moreover, even the cloud parameters are representative of the climatological state, it is simply not possible to derive the climatological temperature field utilizing mechanisms involving only the vertical transport. Obviously, the large scale horizontal transport must also be considered in order to determine reliably the meridional temperature structure.

6. Conclusions

In this paper we have utilized an one-dimensional radiative-convective model to investigate the climatic effects of the cirrus cloud thickness and location embedded in various atmospheric conditions on the thermal equilibrium temperature of the earth's atmosphere. Computations of solar and infrared fluxes and heating and cooling rates are based on the programs developed by Freeman and Liou (1979), Liou and Wittman (1979), and recently by Liou and Ou (1981). These programs carefully take into account the radiative properties of cirrus in the flux calculation. To incorporate the vertical heat transport component in the temperature profile determination, the convective adjustment procedure using a lapse rate of 6.5°C/km outlined by Manabe and Wetherald (1967) is used in conjunction with our cloud-radiation program.

We first find that increasing the water vapor content of the lower atmosphere will increase the temperature of the troposphere and the earth's surface. Numerical experiments were then successively carried out for cirrus clouds of 0.1, 1 and 3 km thickness with bases at 2.5 and 8 km in a tropical atmosphere to study the cloud thickness (or ice content) and location effects on the thermal equilibrium temperature profile. Results show that high clouds (clouds with bases of 8 km) and thin clouds (clouds that are 0.1 km thick) will cause the atmosphere and surface temperatures to be warmer than in the clear case. The degree to which warming occurs in the thin cloud case is on the order of 20°K which is a significant departure from the clear case. On the contrary, cirrus clouds which are both low (cloud bases 2-5 km) and thick (1-3 km thick) will generate cooling effects in the atmosphere and on the surface. The effects of increasing the surface albedo under restricted atmospheric conditions was also studied for clear and cloudy conditions. Results illustrate that higher surface albedos lead to colder temperatures throughout the troposphere. Whether the presence of a cloud will tend to intensify or reduce the cooling below the cloud could not be determined from the limited experiments carried out in this study.

Finally, we have constructed a composite thermal equilibrium temperature profile using the climatological water vapor and ozone profiles and cloud parameters for the tropical atmosphere. Comparison with the climatological temperature profile in the tropics shows differences within about 1°K in the troposphere and of about 10°K in the stratosphere. Additional experiments employing midlatitude and subarctic climatological data are also performed and results indicate that simulated tropospheric temperatures deviate from climatological values by about 5°K. Lastly, using the tropical data, we show that increasing the cirrus cloud cover by 10% will increase the surface temperature by about 0.2°K.

Acknowledgements

This research was supported by the Atmospheric Research Section of the National Science Foundation under Grant ATM78-26259. Most of the computations were done in the National Center for Atmospheric Research located in Boulder, Colorado.

References

Freeman, K. P. and K. N. Liou, 1979: Climatic effects of cirrus clouds. *Advances in Geophys.*, **21**, 231-287.

Liou, K. N., 1973: A numerical experiment on Chandrasekhar's discrete ordinate method for radiative transfer: Applications to cloudy and hazy atmospheres. *J. Atmos. Sci.*, **30**, 1303-1326.

——— and S. C. Ou, 1981: Parameterization of infrared radiative transfer in cloudy atmospheres. *J. Atmos. Sci.*, **38**, (December).

——— and T. Sasamori, 1975: On the transfer of solar radiation in aerosol atmospheres. *J. Atmos. Sci.*, **32**, 2166-2177.

——— and G. D. Wittman, 1979: Parameterization of the radiative properties of clouds. *J. Atmos. Sci.*, **36**, 1261-1273.

London, J., 1957: A study of the atmospheric heat balance. New York University, Final Report, Contract AF19(122)-166, 99 pp.

Machta, L. and T. Carpenter, 1971: Trends in high cloudiness at Denver and Salt Lake City. In "Man's Impact on Climate" (Matthews, W. H., W. W. Kellogg and G. D. Robinson, eds.), MIT Press, Cambridge, Massachusetts, 410-415.

Manabe, S. and R. F. Strickler, 1964: Thermal equilibrium of the atmosphere with a convective

adjustment. *J. Atmos. Sci.*, **21**, 361-385.
———— and R. T. Wetherald, 1967: Thermal equilibrium of the atmosphere with a given distribution of relative humidity. *J. Atmos. Sci.*, **24**, 241-259.
McClatchey, R. A., R. W. Fenn, J. E. Selby, F. E. Voltz and J. S. Garing, 1971: Optical properties of the atmosphere (3rd ed.). AFCRL-72-0497.
Sasamori, T., J. London and D. V. Hoyt, 1972: Radiation budget of the southern hemisphere. *Meteor. Monogr.*, **13**, (35), Ch. 2.
Stephens, G. and P. J. Webster, 1981: Clouds and climate sensitivity of simple systems. *J. Atmos. Sci.*, **38**, 235-247.
Study of Man's Impact on Climate, 1971: *Inadvertent Climate Modification*. MIT Press, Cambridge, Massachusetts.
Telegadas, K. and J. London, 1954: A physical model of the northern hemisphere troposphere for winter and summer. New York University, Sci. Rep. No. 1, Contract AF19(122)-165, 55 pp.
Wallace, J. M. and P. V. Hobbs, 1977: *Atmospheric Science: An Introductory Survey*. Academic Press, New York, 467 pp.

絹雲が存在する大気の熱平衡温度に関する数値実験

Kuo-Nan Liou and Kristi L. Gebhart

Department of Meteorology, University of Utah

地球大気の熱平衡温度に対する種々の大気状態の絹雲の厚さと高度の気候学的影響を研究するために数値実験を行なった。ここで用いた対流調節法は真鍋らによって導入された方法に従ったが，半透明で黒体ではない雲の放射伝達の扱い方に新しい試みをとり入れて，放射対流モデルを作った。このモデルは，絹雲の日射と赤外放射に対する特性が温度分布の決定に関して充分注意深く取扱えるように作られている。その結果，射出率が 0.45 で日射の反射率が 0.08 の 0.1 km の厚さを持つ薄い絹雲が存在すると，大気は絹雲の高度にかかわらず 20°K も加熱されることがわかった。しかし，厚い雲ではその高度が重要になる。低く厚い氷の雲の存在は大気をかなり冷やす効果があり，これは他の研究結果とも一致する。熱帯の大気で，水蒸気とオゾン分布の気候値と雲の統計を用いて，総合的に熱平衡温度分布を計算した。この結果を熱帯の温度分布の気候値と比較すると，対流圏ではよく一致した（1°K 以内）が，成層圏では約 10°K の差異となった。熱帯の例では，晴天部分を減らして絹雲量を10%増加させると，地表温度は約 0.2°K だけ上昇することが明らかになった。